Wideband Dual Segment Cylindrical Dielectric Resonator Antenna Terminated in a Bio-Medium

Ravi Kumar Gangwar, S. P. Singh, D. Kumar[1]

Abstract –**In this paper, a wideband dual segment cylindrical dielectric resonator antenna (CDRA) is proposed for 5 GHz WLAN/WiMAX band. The simulation results for the radiation characteristics of the proposed antenna and the absorbed power distribution in a homogenous bio-medium (muscle layer) in direct contact with the proposed CDRA are reported at different frequencies. The specific absorption rate (SAR) distribution in muscle layer for antenna-to-bio-medium separation of 200 mm is also determined at the antenna resonant frequency of 6.238 GHz. The input characteristics of CDRA are compared with those of single segment CDRA of same size and different material dielectric constants. The simulation study has been carried out using CST Microwave Studio software.**

Keywords –**Dual segment CDRA, radiation characteristics, bio-medium, specific absorption rate, effective field size, penetration depth.**

I. INTRODUCTION

Several investigators have focused attention on Dielectric resonator antennas (DRAs) due to their simple geometry, small size, high radiation efficiency, flexible feed arrangement, wide range of material dielectric constants, ease of excitation and easily controlled characteristics [1-5]. DRAs are available in various basic classical shapes such as rectangular, cylindrical, spherical and hemispherical geometries.

The techniques used for improving the bandwidth of DRA include changing its aspect ratio, varying the dielectric constant of the antenna material and employing multi-segments and stacked DRAs. The DRAs of lower material dielectric constant values are preferred for wideband applications. This results in week coupling. Multi-segment DRAs can be used to overcome this problem [6-7].

With the expansion of current use and anticipated further increases in the use of wireless portable devices, interest in the study of interactions between antennas and human body is growing. These activities are motivated by two factors. First one stems from the need to evaluate the performance of antenna in presence of bio-layers and second one is concerned with the rate of electromagnetic energy absorption, known as specific absorption rate (SAR) [8]. The human body being lossy absorbs certain amount of electromagnetic radiation generated from portable wireless device situated in its vicinity. Therefore, it is of interest to evaluate the power absorbed /specific absorption rate (SAR) distribution in the body tissues due to wireless device antenna radiating electromagnetic waves [9]. The electric field induced and hence SAR within the human body depends on several factors including the strength and frequency of the external field, the shape, size and electrical characteristics of the body tissues and the orientation of the body in relation to the external field.

R. Kumar Gangwar and S.P. Singh are with the Department of Electronic Engineering, Institute of Technology, Banaras Hindu University, Varanasi-221005, India, E-mail: ravi.gangwar.ece07@itbhu.ac.in, spsingh.ece@itbhu.ac.in
[1]D. Kumar is with the Department of Ceramic Engineering of the same Institution E-mail: devendra.cer@itbhu.ac.in

In this paper, design and simulation of a wideband dual segment cylindrical dielectric resonator antenna (CDRA), which is fed by a 50 Ω coaxial probe for 5 GHz WLAN/WiMAX band, is presented. The simulated results for radiation characteristics of the proposed antenna and also the specific absorption rate (SAR) distribution in a homogenous bio-medium (muscle layer) in direct contact with the proposed antenna are reported at different frequencies. The SAR distribution in the bio-medium for antenna-to-muscle layer separation of 200 mm is also evaluated at the antenna resonant frequency. The input characteristics of the proposed CDRA are compared with those of the single segment DRA of same size and different material dielectric constants. The CST Microwave studio software was used to obtain the simulation results.

II. ANTENNA DESIGN

The dual segment CDRA consists of lower segment made from teflon sheet with dielectric constant $\varepsilon_{r1} = 2.1$ and an upper segment of glass ceramic block with $\varepsilon_{r2} = 7.735$ as shown in Fig. 1. The dual segment CDRA is placed on a ground plane of size 60×60×4 mm^3. The lower and upper segments of the CDRA have dimensions of $D\times l$ = *14.15*×10 mm^2 and $D\times l_1$= 14.15×6 mm^2 respectively. The CDRA is assumed to be excited by a 50 Ω coaxial probe of outer radius 2 mm, and inner radius 0.65 mm. The height of the probe is determined through simulation to obtain minimum return loss at the resonant frequency of the antenna. The probe height above the surface of ground plane is found to be 9.5 mm.

The resonant frequency of single segment CDRA excited in $HEM_{11\delta}$ mode can be written as [1], [10]

$$f = \frac{6.324\,c}{2\pi a\sqrt{2+\varepsilon_r}}\left\{0.27 + 0.36\frac{a}{2h} + 0.02\left(\frac{a}{2h}\right)^2\right\} \qquad (1)$$

where $a = \frac{D}{2}$, D is the diameter of CDRA, h is the height of the CDRA above ground plane, c is the velocity of microwave in free space (=3×10^{8}m/sec) and ε_r is the relative permittivity of CDRA material.

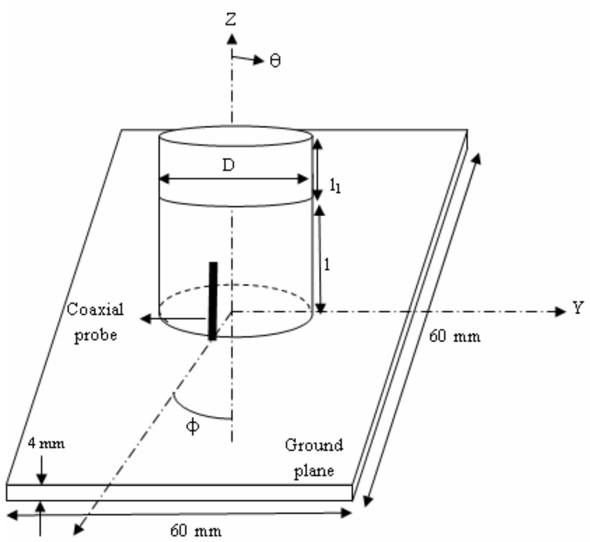

Fig. 1 Geometry of dual segment CDRA

Equation (1) has been obtained through curve fitting and numerical simulations based on the method of moments [1] and [11].

Radiation Q-factor of the isolated cylindrical DRA can be written as [1], [10]

$$Q = 0.01007(\varepsilon_r)^{1.3}\left(\frac{a}{h}\right)\left[1 + 100e^{-\left[2.05\left(\frac{a}{2h}\right) - \frac{1}{80\left(\frac{a}{h}\right)^2}\right]}\right] \quad (2)$$

The percentage bandwidth of the isolated CDRA is given by [1], [10].

$$\% BW = \frac{S-1}{\sqrt{SQ}} \times 100 \quad (3)$$

where S and Q are the VSWR and radiation Q-factor of the isolated CDRA.

Equations (1)-(3) can be used to compute the resonant frequency, radiation Q-factor and bandwidth of the dual segment CDRA by replacing CDRA material dielectric constant, ε_r and height h with their modified values termed as ε_{eff} and h_{eff} respectively. Adopting a simple static capacitance model, the following expression for ε_{eff} and h_{eff} are obtained:

$$\varepsilon_{eff} = \frac{h_{eff}}{\frac{1}{\varepsilon_{r1}} + \frac{1}{\varepsilon_{r2}}}, \text{ and } \quad h_{eff} = l + l_1 \quad [6], [12]$$

where l and l_1 are the length of lower and upper segments of CDRA respectively.

The resonant frequency, Q-factor and bandwidth of the dual segment CDRA computed using equations (1), (2) and (3) are found to be 6.225 GHz, 1.6644 and 42.4842% respectively.

III. Result and Discussion

A. Return loss and Input Impedance Characteristics

The simulation study of return loss and input impedance versus frequency characteristics of the proposed probe excited dual segment CDRA has been carried out using CST Microwave Studio software. The simulated return loss and input impedance versus frequency curves of the proposed antenna have been presented respectively in Figs. 2 and 3. From Fig. 2 the resonant frequency, operating frequency range and the percentage bandwidth of the CDRAs are extracted and the results are shown in Table 1. The theoretical values of resonant frequency and the percentage bandwidth of the dual segment CDRA computed using equations (1) and (3) are in good agreement with simulated values.

From Fig. 2 and Table 1, it can be seen that the proposed CDRA provides wide bandwidth and covers 5 GHz WLAN/WiMAX band.

It is worth mentioning that the input resistance at resonant frequency of the proposed CDRA is found to be 51.54 Ω providing very good impedance match to 50 Ω coaxial feeder. From Fig. 3 it can be observed that the frequency at which total reactance of the structure is zero does not coincide with maximum-resistance frequency. This might have happened due to finite reactance offered by the coaxial probe feed.

Fig. 4 shows the return loss versus frequency characteristics for different lengths of the upper segment keeping total antenna height constant at 16 mm. From Fig. 4 it can be seen that the bandwidth of the antenna increases with the upper segment length. This occurs due to the fact that, the dominance of electric field in the lower segment having lower dielectric constant value increases with upper segment length. Therefore, effective surface area-to-volume ratio of the antenna increases with upper segment length which reduces the Q-factor and increases the antenna bandwidth.

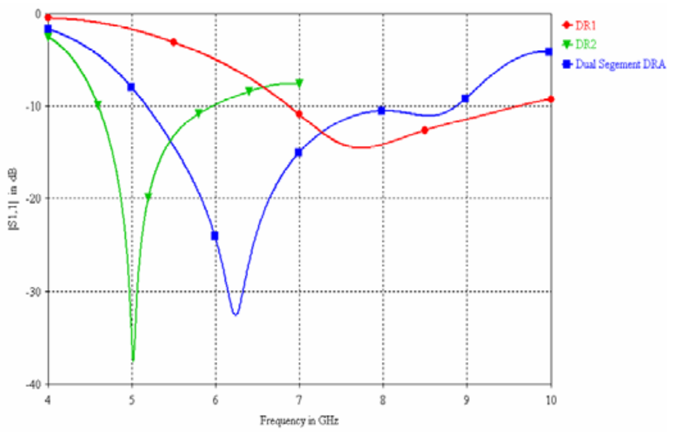

Fig. 2 Return loss versus frequency performance of dual segment CDRA

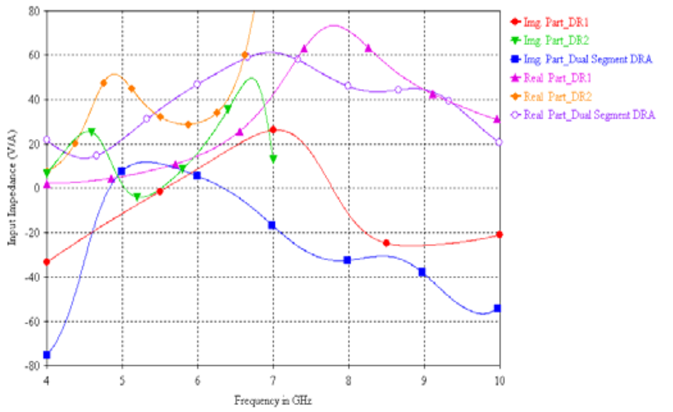

Fig. 3 Input impedance versus frequency curves of dual segment CDRA

It can be also noted from Fig. 4 that the resonant frequency of the antenna first decreases and then increases with upper segment length. The trend of variation in resonant frequency of the antenna with upper segment length can be explained on the ground similar to that said earlier i.e. electric field strength in the lower segment having lower dielectric constant value increases with upper segment length but the rate of change of electric field strength (in lower segment) with upper segment length becomes significant in later phases, though it is negligible in initial phase. Therefore, as upper segment length is increased, this segment dominates in initial phase to provide higher antenna effective volume and hence lower resonant frequency. But in later phases, lower segment having lower ε_r value dominates due to prominence of electric field in this region, thereby reducing antenna effective volume and increasing its resonant frequency.

A1. Performance comparison of single and dual segment CDRAs

The return loss and input impedance characteristics of single segment DRAs of same size as the dual segment CDRA are also obtained through simulation. The first single segment DRA has material dielectric constant of 2.1, whereas the second one has material dielectric constant of 7.735. The simulated values of return loss and input impedance versus frequency for single segment CDRAs are shown in Figs. 2 and 3 respectively along with the corresponding characteristics for dual segment CDRA. The return loss parameters for single segment CDRAs are extracted from Fig. 2 and the results are provided in Table 1.

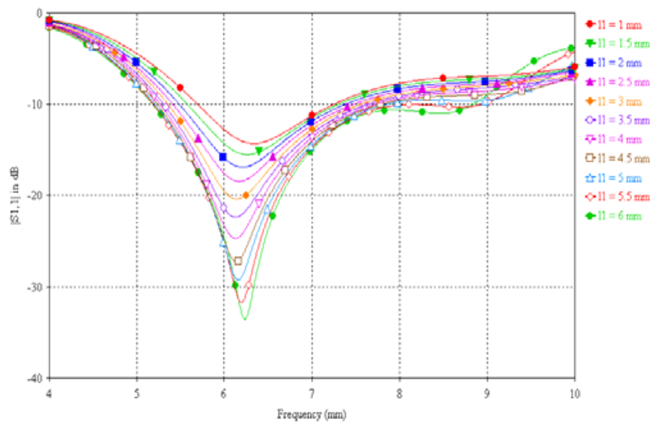

Fig. 4 Effect of variation in length of upper dielectric segment on the return loss versus frequency characteristics of dual segment CDRA

TABLE 1
RETURN LOSS PERFORMANCE

Parameters	Dual Segment CDRA	DR1 ($\varepsilon_{r1} = 2.1$)	DR2 ($\varepsilon_{r2} = 7.735$)
Resonant frequency in GHz	6.238	7.732	5.02
Operating frequency range in GHz ($\lvert S_{11}\rvert = 10dB$)	5.182 -8.836	6.885 – 9.952	4.604 – 5.954
Return loss bandwidth in %	58.576 %	39.66 %	26.89 %

From Fig. 2 and Table 1, it can be observed that dual segment CDRA provides wider bandwidth in comparison to single segment CDRAs with different material dielectric constants. Also, the values of resonant frequency and bandwidth of single segment CDRA having material ε_r value of 2.1 are higher as compared with the antenna with material ε_r value of 7.735. The trend of variation in resonant frequency can be explained on the basis of change in effective volume with increase in material dielectric constant. The effective antenna volume increases with material ε_r value of the antenna and hence resonant frequency reduces with increase in ε_r value. The increase in bandwidth may be due to increase in effective surface area-to-volume-ratio of the antenna with reduction in material ε_r of the antenna which increases the loss due to radiation from the antenna thereby reducing its radiation Q-factor.

From Fig. 3 it can be seen that the value of input resistance at resonant frequency of the single segment CDRAs are also in good impedance match with 50 Ω coaxial feeder. The frequency at which total reactance of each single segment CDRA is zero does not coincide with maximum-resistance frequency due to the reason identical to that given in paragraph 3 of Section III-A.

B. Near Field Distribution

The simulation study of electric field distribution in the proposed dual segment wideband CDRA has been carried out at the resonant frequency of 6.238 GHz. When proposed antenna is excited using a 50 Ω coaxial probe as shown in Fig. 1, the electric field distribution in x-z plane looks like that shown in Fig. 5. It is apparent from Fig. 5 that the coaxial probe excites $HEM_{11\delta}$ dominant mode field in the structure.

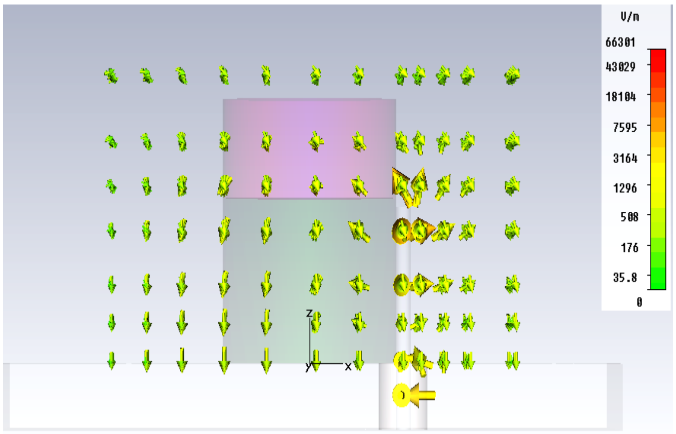

Fig. 5 Electric field distribution in dual segment CDRA

C. Far Field Performance

The simulation results for far-field characteristics of the proposed dual segment CDRA were obtained at resonant frequency of 6.238 GHz and at four other representative frequency of 5.2 GHz, 5.5 GHz, 5.8 GHz and 6.6 GHz within the -10 dB return loss bandwidth of the antenna.

The simulated radiation patterns of the proposed antenna in X-Z, Y-Z and X-Y planes, and in three-dimensions at 6.328 GHz are shown in Figs. 6 (a), (b), (c) and (d) respectively. The far-field patterns of the antenna at other frequencies are not shown here for brevity. The far-field parameters of the proposed antenna are extracted from Fig. 6 and results are shown in Table 2. The parameters of the antenna in X-Y plane are not provided in Table 2 because the radiation pattern of the antenna in this plane at each of the five frequencies is omni-directional.

The simulated values of directivity, gain and total efficiency of the antenna at different frequencies are also given in Table 2.

From Table 2 it can be observed that the 3 dB angular widths of the proposed antenna in both X-Z and Y-Z planes decrease with increasing frequency. It is also noted from Table 2 that the values of gain and directivity of the antenna increases with frequency, while total efficiency first increases, reaches the maximum at the resonant frequency and then goes down. The gain and directivity of the antenna are found to match the characteristics of wideband antenna used for WLAN and WiMAX applications [13-14].

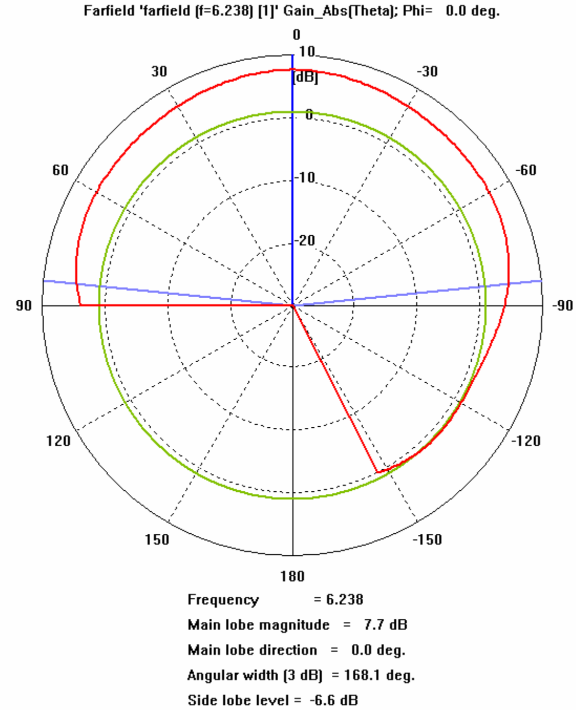

(a)

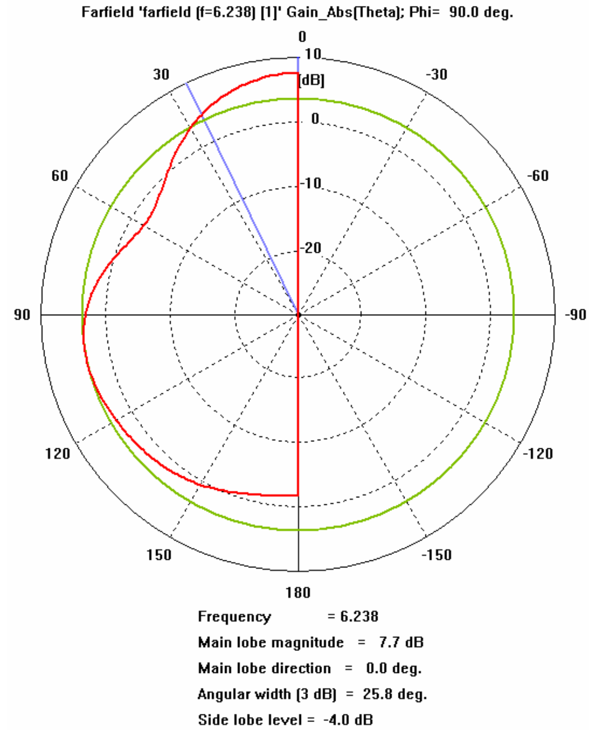

(b)

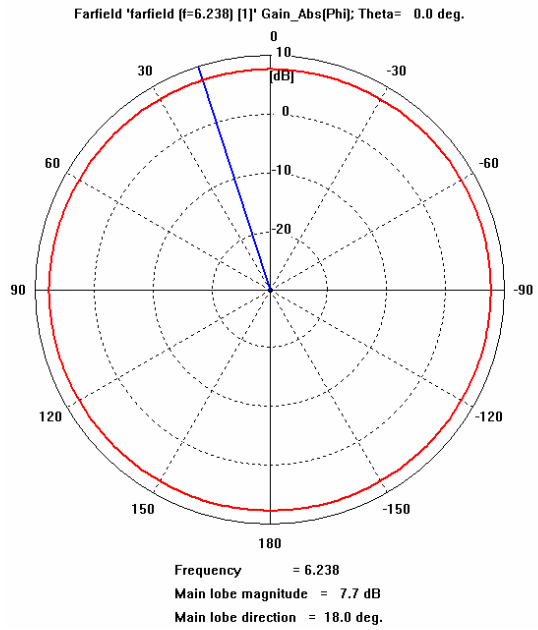

(c)

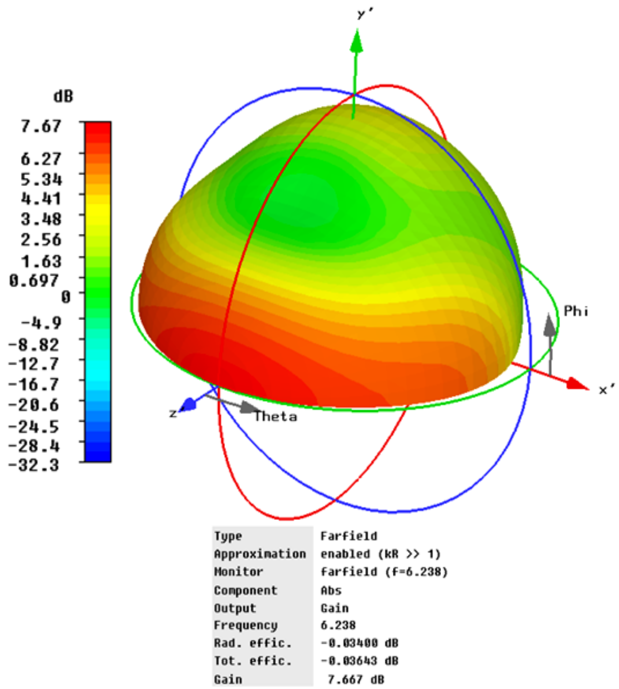

(d)

Fig. 6 Far field patterns of dual segment CDRA (a) in X-Z plane (b) in Y-Z plane (c) in X-Y plane (d) 3-D pattern

D. SAR Evaluation

The specific absorption rate (SAR) is defined as the amount of power absorbed per unit mass of the tissue. The origin of coordinate system was selected on the top surface of ground plane coinciding with the central line of dual segment CDRA as shown in Fig. 7 for simulation of SAR distribution. The power fed to the antenna was initially assumed to be 0.2 W. The simulated SAR (10g) distributions in the muscle layer of size 10×10×12 cm^3 in direct contact with the proposed antenna of original dimensions along X, Y and Z directions at the resonant frequency of 6.238 GHz and at other frequencies 5.2 GHz (low & mild U-NII band 5.15-5.35 GHz), 5.5 GHz (WRC band 5.47-5.725 GHz), 5.8 GHz (upper U-NII/ISM band 5.725-5.85 GHz) and 6.6 GHz are shown in Fig. 8. The simulation of SAR distribution in a homogenous bio-medium, for antenna-to-bio-medium separation of 200 mm was also carried out at the antenna resonant frequency of 6.238 GHz assuming input power of 0.2 W and the results are shown in Fig. 9. The mass density of muscle layer available in the literature is 1050 Kg/m^3[15]. The complex permittivity, electrical conductivity and loss tangent values of muscle layer compiled from the available literature [16] at different frequencies are shown in Table 3.

The three parameters of importance for obtaining the amount of power absorbed and the volume of the tissue absorbing significant amount of power are SAR, effective field size (EFS) and penetration depth. The EFS is defined as the area that is enclosed within the 50% SAR contour inside the tissue. The EFS provides the resolution of the antenna in transverse directions. The penetration depth is the depth at which SAR becomes 1/ e^2 of its value at the surface [15].

The maximum SAR (10g), EFS and penetration depth in the bio-medium due to the dual segment RDRA extracted from Fig. 8 are shown in Table 4. The effect of change in power fed to the antenna on SAR distribution in the bio-medium has also been studied by reducing the power from 0.2 W to 0.02 W. Table 4 also shows maximum value of SAR (10g) in the bio-medium due to the antenna with input power of 0.02 W.

From Table 4 it can be observed that maximum value of SAR (10g) increases with frequency. The EFS value decreases with increase in frequency. The penetration depth value reduces with increase in frequency. The trend of changes in EFS value and penetration depth in muscle may be due to increase in the conductivity of the bio-medium with frequency and frequency dependent characteristics of the antenna. It is also noted from Table 4 that maximum value of SAR (10g) in muscle layer reduces in proportion to decrease in power fed to the antenna, but other parameters (EFS and penetration depth) remain unchanged.

From Fig. 9 it can be observed that the SAR (10g) distribution covers larger cross-sectional area (though at reduced strength) with greater antenna-to-bio-medium separation due to more beam spread. From this figure the penetration depth for antenna-to-bio-medium separation (d) of 200 mm is found to be 58.58 mm.

It is noted that penetration depth at larger antenna-to-muscle layer separation is higher. This has happened due to better coherency among the waves before entering the bio-medium at greater separation.

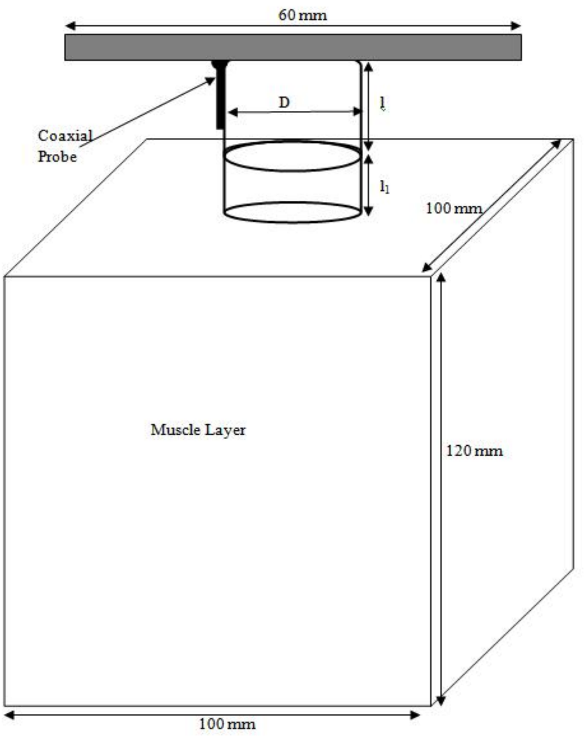

Fig. 7 Dual segment CDRA in direct contact with muscle layer

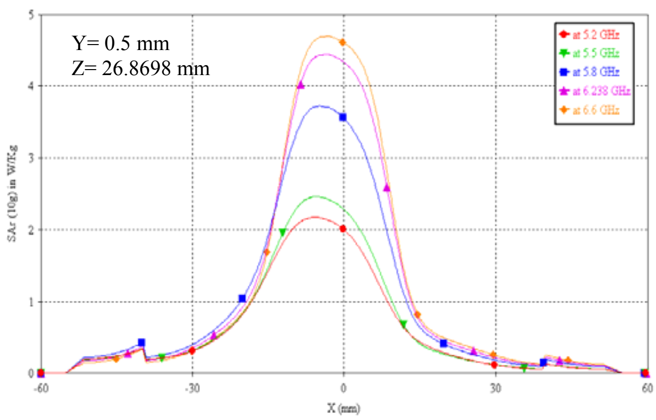

(a)

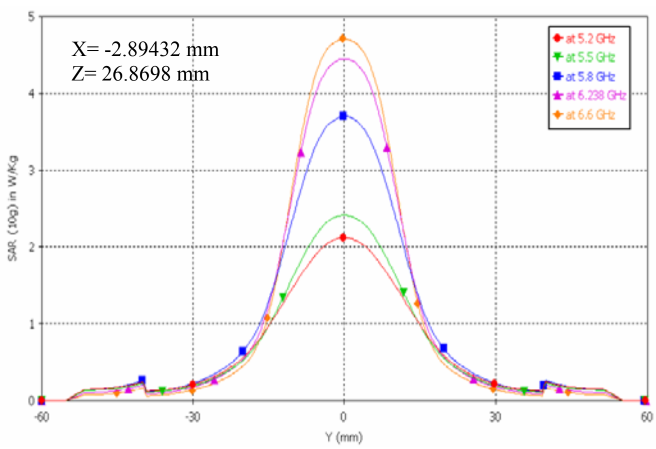

(b)

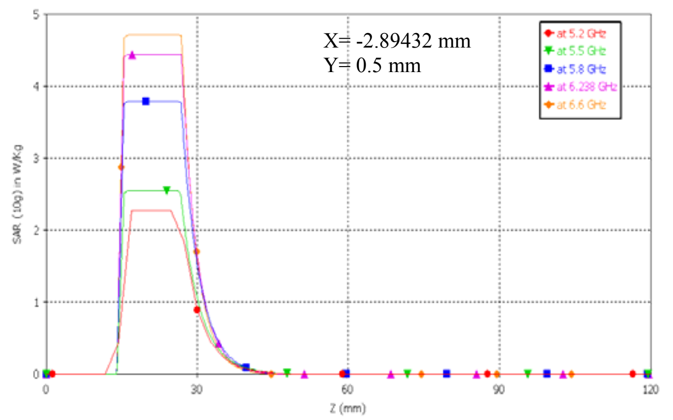

(c)

Fig. 8 Variation of SAR (10g) in muscle layer in direct contact with the dual segment CDRA with distance along (a) X-direction, (b) Y-direction, and (c) Z-direction for different frequencies

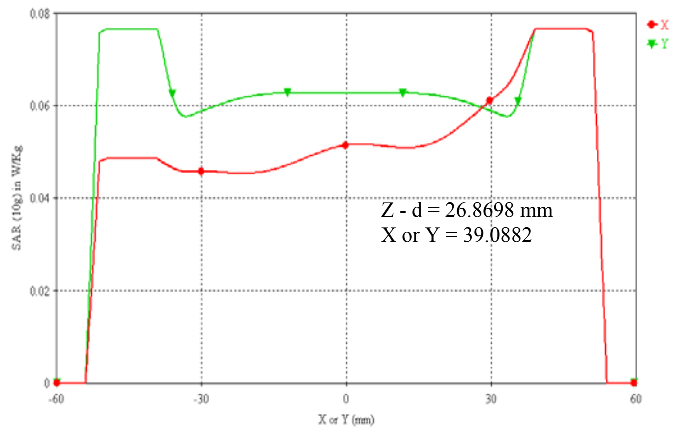

(a)

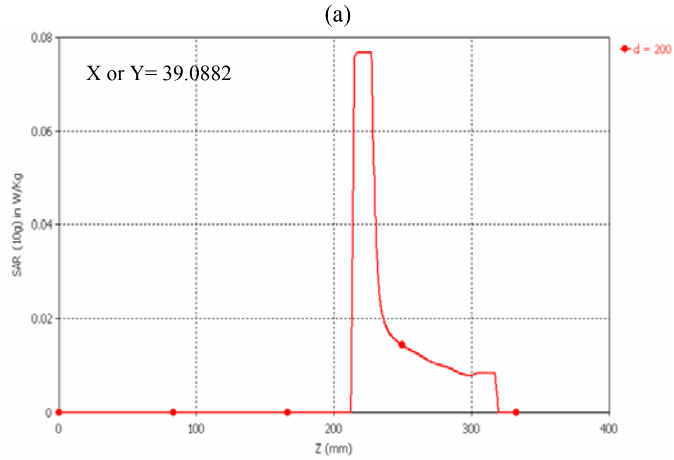

(b)

Fig. 9 Variation of SAR (10g) at resonant frequency of dual segment CDRA with distance along (a) X-direction or Y-direction (b) Z-direction for antenna-to-bio-medium separation of 200 mm

IV. Conclusion

A wideband dual segment cylindrical DRA for 5 GHz WLAN/WiMAX band has been proposed in this paper. The radiation characteristics of the proposed antenna and SAR distributions in a homogenous muscle layer in direct contact with the antenna have been evaluated at different

WLAN/WiMAX frequencies through simulation studies using CST Microwave Studio software. The SAR distribution in muscle layer for antenna-to-muscle layer separation of 200 mm has also been determined through simulation at the antenna resonant frequency. The input characteristics of the proposed antenna have also been compared with single segment DRA of same size as the proposed antenna. From the study it is inferred that the bandwidth of the proposed antenna is found to be 58.576%, which covers 5 GHz WLAN/WiMAX band and is much greater than single segment antenna bandwidth. The gain and total efficiency of the proposed antenna remains above 6.5 dB and 90% respectively throughout WLAN/WiMAX band. The value of SAR in the bio-layer increases with frequency. Also, reduction in penetration depth and improvement in transverse plane resolution have been noticed with increase in frequency. The value of SAR (10g) reduces when antenna input power is lowered whereas the resolutions of the antenna along X, Y and Z directions are not affected by change in input power. The results presented here may find potential application in wireless communication field for designing a wideband antenna and evaluating the power absorption in bio-layers due to the antenna.

TABLE 2

FAR FIELD PARAMETERS OF DUAL SEGMENT CDRA

Far field parameters		At 5.2 GHz	At 5.5 GHz	At 5.8 GHz	At 6.238 GHz	At 6.6 GHz
Directivity in dBi		6.708	6.985	7.258	7.701	8.141
Gain in dB		6.680	6.961	7.232	7.667	8.111
Total efficiency in %		90.04	95.75	98.23	99.16	98.51
3-dB Beam-width in deg.	(Y-Z plane)	31.2	29.5	28.1	25.8	23.8
	(X-Z plane)	203.8	192.8	184.4	168.1	152.1
Side lobe level in dB	(Y-Z plane)	-3.0	-4.4	-4.4	-4.0	-4.1
	(X-Z plane)	-3.3	-4.5	No side lobe	-6.6	-6.4

TABLE 3

DIELECTRIC PROPERTIES OF MUSCLE LAYER

Parameters	At 5.2 GHz	At 5.5 GHz	At 5.8 GHz	At 6.238 GHz	At 6.6 GHz
Dielectric Constant	49.278	48.883	48.485	47.898	47.409
Electrical Conductivity (S/m)	4.2669	4.609	4.915	5.4931	5.9465
Loss Tangent	0.29932	0.30815	0.31715	0.33048	0.34162

TABLE 4

SAR PERFORMANCE OF DUAL SEGMENT CDRA IN MUSCLE LAYER

Parameters		At 5.2 GHz	At 5.5 GHz	At 5.8 GHz	At 6.238 GHz	At 6.6 GHz
Maximum SAR (10g)	0.2W	2.28017 W/Kg	2.54492 W/Kg	3.79065 W/Kg	4.44155 W/Kg	4.71106 W/Kg
	0.02W	0.228017 W/Kg	0.254492 W/Kg	0.379065 W/Kg	0.444155 W/Kg	0.471106 W/Kg
Effective Field Size		25.56×28.36 mm^2	24.75×26.42mm^2	21.6×24.76 mm^2	22.24×23.30 mm^2	22.98×22.73 mm^2
Penetration Depth		18.3 mm	18.29 mm	17.8 mm	17.1 mm	16.59 mm

ACKNOWLEDGEMENT

First author, Ravi Kumar Gangwar wishes to acknowledge to the Department of Electronics Engineering, IT-BHU, Varanasi and UGC, New Delhi for awarding Senior Research Fellowship. Authors wish to thank the editorial board and reviewers for their invaluable suggestions to improve the quality of the paper.

REFERENCES

[1] R.K. Mongia and P. Bhartia, "DRA- A review and general design relation for resonant frequency and bandwidth," *International journal of Microwave and Millimeter Wave Computer –aided Engineering*, vol.4, No.3, pp 230-247, 1994.

[2] Ittipiboon and R. K. Mongia, "Theoretical and experimental investigations on rectangular dielectric resonator antennas," *IEEE Transactions on Antennas and Propagation,* Vol. 45, No. 9, pp. 1348– 1356, Sept. 1997.

[3] P.Rezaei, M.Hakkak and K.Forooaghi, **"**Design of wideband dielectric resonator antenna with a two segment structure**,"** *Progress in Electromagnetics Research*, PIER 66, pp. 111–124, 2006.

[4] Darko Kajfez and A. A. Kishk, "Dielectric Resonator Antenna- Possible Candidate for Adaptive Antenna Arrays," *Proceedings VITEL 2002, International Symposium on Telecommunications, Next Generation Networks and Beyond*, Portoroz, Slovenia, May 13-14, 2002.

[5] M. Saed and R. Yadla, "Microstrip-fed low profile and compact dielectric resonator antennas," *Progress In Electromagnetics Research*, PIER 56, pp.151–162, 2006.

[6] Aldo Petosa, "Dielectric Resonator Antennas Handbook,*"* Artech House, Boston, London, 2007.

[7] Yuehe Ge, K.P. Esselle "A dielectric resonator antenna for UWB applications," *IEEE International Symposium on Antennas and Propagation Society*, pp.1-4, 1-5 June 2009.

[8] Michal Okoniewski, Maria A. Stuchly, "A study of the handset antenna and human body interaction," *IEEE Trans. on Microwave Theory and Techniques*, vol. 44, no. 10, pp.1855-1864, 1996.

[9] Pradier , D. Lautru, M. F. Wong, V. H. Fouad and J. Wiart, "Rigorous evolution of specific absorption rate (SAR) induced in a multilayer biological structure," *European Microwave Conference,* Vol. 3, 2005.

[10] A. A. Kishk, A. W. Glisson, and G.P. Junker, "Study of broadband dielectric resonator antennas," *Antenna Application Symposium*, pp. 45-68, 1999.

[11] A. A. Kishk, A. W. Glisson and D. Kajfez, Computed resonant frequency and far fields of isolated disks, IEEE Antennas Propogat. Soc. Int. Symp. Dig. (1993), 408-411.

[12] K. M Luk and K. W. Leung, "Dielectric Resonator Antennas" Research Study Press Hertfordshire, England, UK, 2002.

[13] Ravi Kumar Gangwar, S.P. Singh and D. Kumar, "A Modified Fractal Rectangular Curve Dielectric Resonator Antenna for WiMAX Application," *Progress in Electromagnetics Research C*, Vol. 12, 37-51, 2010.

[14] Tze-Hsuan Chang and Jean-Fu Kiang, "Sectorial-beam dielectric resonator antenna for WIMAX with bent ground plane," *IEEE Transactions on Antennas and Propagation,* Vol. 57, No. 2, pp. 563– 567, Feb. 2009.

[15] M. A. Ebrahimi-Ganjeh, "Study of Water Bolus Effect on SAR Penetration Depth and Effective Field Size for Local Hyperthermia," *Progress in Electromagnetics Research,* vol. 66, pp.111–124, 2006.

[16] An Internet resource for the calculation of the Dielectric properties of Body tissues in the frequency range 10Hz-100GHz. Italian national research council, institute for applied physics. http://niremf.ifac.cnr.it/tissprop/